Ethylene adsorption on $Pt/Au/SiO_2$ catalysts

Jianyi Shen [a,b], Josephine M. Hill [a], Ramchandra M. Watwe [a], S.G. Podkolzin [a] and J.A. Dumesic [a,*]

[a] *Department of Chemical Engineering, University of Wisconsin-Madison, Madison, WI 53706, USA*
[b] *Department of Chemistry, Nanjing University, Nanjing 210093, China*

Received 22 February 1999; accepted 26 April 1999

Ethylene adsorption on a $Pt/Au/SiO_2$ catalyst (2 wt% Pt; Au/Pt atomic ratio of 10) was studied using adsorption microcalorimetry and FTIR spectroscopy. Ethylene adsorption at 300 K on $Pt/Au/SiO_2$ produced π-bonded, di-σ-bonded, and ethylidyne species with an initial heat of 140 kJ/mol, compared to a heat of 157 kJ/mol for Pt/SiO_2 on which only ethylidyne species formed. At 203 and 263 K, ethylene adsorbed on Pt as well as on Au surface atoms for the $Pt/Au/SiO_2$ catalyst. Quantum chemical, DFT calculations indicate that Au exerts a significantly smaller electronic effect on Pt than does addition of Sn to Pt.

Keywords: microcalorimetry, IR, platinum, gold, ethylene, CO, adsorption, quantum chemical calculations, DFT

1. Introduction

In previous studies, our group has investigated the role of tin in modifying Pt/SiO_2 catalysts for isobutane dehydrogenation [1–4] and for ethylene and acetylene adsorption [5,6]. Our results indicate that Sn exerts both a geometric and an electronic effect on Pt. In particular, Sn forms a substitutional alloy with Pt and thereby decreases the size of surface Pt ensembles (geometric effect); and, Sn donates electrons to Pt thereby altering the adsorption characteristics of the catalyst (electronic effect). For example, the formation of ethylidyne species from ethylene adsorption on Pt surfaces requires three-fold hollow sites composed of adjacent Pt atoms, and Sn prevents the formation of ethylidyne species by decreasing the number of these sites [5,7]. In addition, our recent work using microcalorimetric measurements and quantum chemical calculations employing density functional theory (DFT) has shown that Sn also weakens the bonding of ethylidyne species at three-fold hollow sites composed of three adjacent Pt atoms surrounded by Sn atoms [5]. These results are supported by TPD studies of ethylene desorption from Pt and Pt/Sn surfaces [7–9].

In contrast to the behavior of Sn, the addition of Au to Pt has been found to exert only a geometric effect on the adsorption of hydrocarbons on Pt [10–14]. For example, the addition of Au to Pt catalysts has been shown to improve the selectivities for the isomerization of n-pentane to isopentane [14], the isomerization of n-hexane to 2- and 3-methylpentane [12,14,15], and the isomerization of neopentane to isopentane and n-pentane [11,13,16]. In each case, the increased selectivity after the addition of Au was attributed to a decrease in the size of the surface Pt ensembles.

In the present paper, we have studied a $Pt/Au/SiO_2$ catalyst using the same techniques that we used previously to study $Pt/Sn/SiO_2$ catalysts, with the aim of comparing the effects of Au and Sn for supported Pt catalysts. Specifically, we have investigated the adsorption of ethylene on $Pt/Au/SiO_2$ catalysts using microcalorimetry and infrared spectroscopy at 300, 263 and 203 K, and quantum chemical calculations employing density functional theory (DFT). We have compared these results to the behavior of Pt and $Pt/Sn/SiO_2$ catalysts [5].

It can be difficult to prepare Pt/Au catalysts because of the miscibility gap in solid solutions of these two metals, between 18 and 98% Pt [17]. Therefore, we have used IR spectroscopy to monitor CO adsorption at low temperatures (203 K) on $Pt/Au/SiO_2$ catalysts to assess separately the numbers of surface Pt and Au atoms, since infrared spectroscopy of adsorbed CO has been used to characterize the surface properties of metal alloy catalysts [18–21]. In addition, we have characterized the Pt/Au catalysts using transmission electron microscopy (TEM) and X-ray diffraction (XRD). We have also used isobutane dehydrogenation as a probe reaction for the interaction between Pt and Au.

2. Experimental

2.1. Catalyst preparation and treatment

Tetraammineplatinum(II) nitrate (Aldrich) and hydrogen tetrachloroaurate(III) hydrate (Aldrich) were used for impregnation of silica (Cab-o-Sil, Cabot Co.) to prepare Pt/SiO_2 and Au/SiO_2 catalysts, respectively. Hydrogen hexachloroplatinate(IV) hydrate (Aldrich) and hydrogen tetrachloroaurate(III) hydrate (Aldrich) were used in a coimpregnation method for the preparation of the $Pt/Au/SiO_2$ catalyst. The required amount of each chemical was dissolved in water, and silica was then added to the aqueous solution to form a gel upon stirring. The gel was dried at room temperature for one day and further dried at 393 K overnight. The Pt/SiO_2 catalyst was calcined

* To whom correspondence should be addressed.

Table 1
Composition and initial heats of ethylene adsorption for catalysts.

Catalyst	Pt loading (wt%)	Au or Sn[a] loading (wt%)	Initial heat for C_2H_4 adsorption[b] (kJ/mol)			
			300 K	263 K	233 K	203 K
Pt/SiO_2	5.6	–	157	135	125	125
$Pt/Au/SiO_2$	1.76	17.17	140	105		100
Au/SiO_2	–	9.78	52			
$7Pt/Sn/SiO_2$	6.2	0.5	135	113	106	106
$3Pt/Sn/SiO_2$	8.1	1.6	129	108	98	98

[a] Results for Pt and Pt/Sn catalysts from [5].
[b] This heat of adsorption is defined as the negative of the enthalpy change of adsorption per mole of gas adsorbed.

in O_2 at 573 K for 4 h. The Au and $Pt/Au/SiO_2$ catalysts were not calcined before reduction. The compositions (Galbraith Laboratories Inc.) of all catalysts are given in table 1. The atomic ratio of Pt : Au in the $Pt/Au/SiO_2$ catalyst is ca. 1 : 10.

Sample treatments for microcalorimetric experiments were performed in a down-flow Pyrex treatment cell. A Pyrex NMR tube (Wilmad Glass) with an outer diameter of 5 mm and length of 18 cm was sealed to the side of a glass treatment cell and served as a capsule in which to seal the samples. The sample was heated in flowing (300 cm^3/min) ultrahigh-purity hydrogen (99.999%, Liquid Carbonic) to 723 K over 8 h, held at 723 K for 8 h, after which time the H_2 was evacuated and the sample was purged in ultrahigh-purity helium (99.999%, Liquid Carbonic) for 2 h. Finally, the sample was sealed in He in the capsule, and this capsule was subsequently loaded into the calorimetric cells.

2.2. Catalyst characterization

Transmission electron microscopy (TEM) measurements were performed with a Phillips CM200 microscope equipped with a LaB_6 filament to determine metal particle sizes. X-ray diffraction (XRD) measurements were performed on a Scintag PadV X-ray diffractometer using Cu Kα radiation with a scan rate of 1.0°/min. X-ray photoelectron spectroscopy (XPS) analysis for the detection of residual chlorine was performed on a Perkin–Elmer Phi 5400 ESCA system equipped with a Phi 5000 spherical capacitor analyzer and using Mg Kα radiation (15 kV, 20 mA and 45° TOA).

2.3. Kinetic experiments

Reaction kinetic studies of isobutane conversion were conducted using a stainless-steel apparatus and a quartz reactor. Helium (Liquid Carbonic) was employed as a carrier gas, and it was purified by passage through copper turnings at 423 K, followed by activated molecular sieves (13X) at 77 K. Isobutane (Liquid Carbonic, 99.5%) was treated by passage over beds of reduced Oxytrap (Alltech) and reduced Ni/alumina at 333 K. Hydrogen (Liquid Carbonic) was treated by passage through a Deoxo unit (Engelhard) and a bed of molecular sieves (13X) at 77 K. The reactor inlet and outlet gases were analyzed by an HP-5890 gas chromatograph with an FID detector and a 10 foot 15% Squalene Chromsorb PAW column at 323 K.

2.4. Microcalorimetric measurements

Microcalorimetric measurements were performed at temperatures from 203 to 300 K using a Setaram BT2.15D heat-flux microcalorimeter. The calorimeter was connected to a gas-handling system and a volumetric system employing Baratron capacitance manometers for precision pressure measurement ($\pm 0.5 \times 10^{-4}$ Torr).

The calorimetric procedures used in this study have been described in detail elsewhere [22,23]. Briefly, each sample was treated *ex situ* in ultra-pure flowing gases and subsequently sealed in a Pyrex capsule, as described above. This capsule containing the sample was then broken in a special set of calorimetric cells [23] after the sample had attained thermal equilibrium with the calorimeter. After the capsule had been broken, the microcalorimetric data were collected by sequentially introducing small doses (1–10 μmol) of probe molecules (H_2, CO or C_2H_4) onto the sample until it became saturated. The resulting heat response for each dose was recorded as a function of time and integrated to determine the energy released (mJ). The amount of gas adsorbed (μmol) was determined volumetrically from the dose and equilibrium pressures and the system volumes and temperatures. The differential heat (kJ/mol), defined as the negative of the enthalpy change of adsorption per mole of gas adsorbed, was calculated for each dose by dividing the heat released by the amount adsorbed.

2.5. Infrared spectroscopic measurements

The design of the infrared spectroscopic cell used in these studies has been described in detail elsewhere [5]. Briefly, this cell allows the sample to be pretreated in flowing gases at temperatures up to ca. 750 K, followed by evacuation of the cell and subsequent dosing of adsorbate gases onto the sample at temperatures from 150 to 750 K. Infrared spectra were typically collected before and after the sample was exposed to an adsorbate, allowing difference spectra to be determined. In this manner, the results from the IR spectroscopy can be used directly to probe the

species formed during microcalorimetric measurements at a specific temperature.

Catalyst samples (about 20 mg) were pressed into self-supporting pellets (13 mm in diameter) and loaded into the IR cell, where they were reduced in flowing H_2 for 8 h at 723 K and then purged in flowing He for 2 h at 723 K. The IR cell was then placed in the chamber of the infrared spectrometer (Mattson Galaxy Series FTIR 5000) and connected to a high-vacuum system. The cell was evacuated to ca. 0.2 Torr He inside the cell to facilitate heat conduction during cooling to sub-ambient temperatures. After the sample pellet cooled to the desired temperature, an IR spectrum for the clean sample was collected. Next, a known amount of CO or ethylene (0.2–2 μmol) was dosed onto the pellet and a spectrum of the sample plus absorbate was collected. Since all dosed molecules were adsorbed, it was not necessary to evacuate the cell prior to collection of spectra. All results reported herein are difference spectra, corresponding to the IR spectrum of the sample with the adsorbate minus the IR spectrum of the sample at the same temperature. Infrared spectra were collected in the absorbance mode with a resolution of 2 cm^{-1}.

Ethylene (99.9%, Matheson) used for both microcalorimetric adsorption and IR spectroscopic studies was purified by successive freeze/pump/thaw cycles with liquid nitrogen.

2.6. Quantum chemical calculations

Quantum chemical DFT calculations were performed on DEC workstations with Jaguar software (Schrödinger, Inc.) [24]. The chosen DFT method uses a hybrid method employing Becke's three-parameter approach, B3LYP [25]. This functional combines the exact HF exchange, Slater's local exchange functional, Becke's 1988 non-local gradient correction to the exchange functional, with the correlation functionals of Vosko–Wilk–Nusair (VWN) and Lee–Yang–Parr (LYP).

The basis set employed in the calculations (LACVP**) uses an effective core potential on all Pt atoms and was developed at Los Alamos National Laboratory by Hay and Wadt [26]. The electrons treated explicitly on Pt are the outermost core and valence electrons ($5s^2\,5p^6\,5d^9\,6s^1$). The C and H atoms were treated with the 6-31G** basis set [27], with all electrons being treated explicitly.

The electronic energy change of adsorption, ΔE_{ads}, is defined as

$$\Delta E_{\text{ads}} = E_{\text{cluster/adsorbate}} - (E_{\text{cluster}} + E_{\text{adsorbate}}),$$

where $E_{\text{cluster/adsorbate}}$ is the electronic energy of adsorbate on the cluster, E_{cluster} is the electronic energy of the bare cluster and $E_{\text{adsorbate}}$ is the electronic energy of the adsorbate.

One of the limitations of cluster calculations is the dependence of the calculated change in electronic energy on the shape and size of the cluster. We have performed DFT calculations using two scenarios to address this cluster size effect on the calculated energies. From our results, it can be noted that while the two scenarios give different values for the change in electronic energy for adsorption, both scenarios predict the same effect for the addition of Au to Pt.

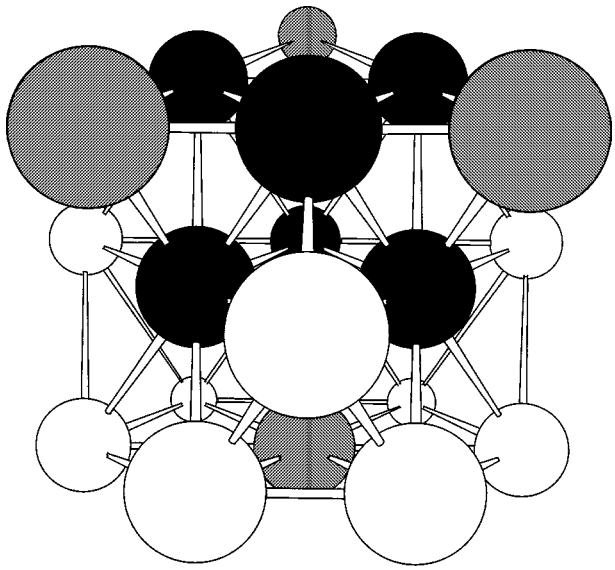

Figure 1. Ball and stick model of the 19-atom cluster used for DFT calculations; dark-shaded circle = Pt atom from 10-atom cluster, light-shaded circle = Pt or Au atom from 10-atom cluster and open circle = Pt atom added to make 19-atom cluster.

In the first scenario for DFT calculations, we studied the interaction of ethylene with constrained, 19-atom Pt clusters. The Pt_{19} cluster was constructed from a Pt_{10} cluster comprised of three layers containing 6, 3, and 1 Pt atoms (see figure 1). These layers correspond to (111) planes stacked in the ABC arrangement of the bulk FCC crystal structure. The nearest-neighbor distances between metal atoms were constrained to be equal to the bulk value of 2.77 Å. The Pt_{19} cluster was then constructed from these same three layers, with additional atoms being added to the second and third layers such that the three layers contain 6, 6, and 7 Pt atoms. Geometry optimizations were conducted for π-bonded ethylene, di-σ-bonded ethylene, and ethylidyne species on constrained Pt_{10} clusters. The additional 9 Pt atoms were then added to the second and third layers of Pt_{10} clusters to make constrained Pt_{19} clusters, and single-point energy calculations were conducted on these clusters containing π-bonded ethylene, di-σ-bonded ethylene, and ethylidyne species. The effects of Au on the adsorptive properties were probed by conducting calculations using a $Pt_{15}Au_4$ cluster formed by replacing the three corners of the 6-atom top layer and the central atom in the bottom layer with Au atoms. The Pt atom in the bottom layer was replaced by a Au atom to give the overall cluster a singlet multiplicity.

In the second scenario for DFT calculations, we studied the interaction of ethylene with fully-optimized, 10-atom Pt clusters. The details of these calculations can be found elsewhere [28]. In this approach, the entire cluster was optimized, i.e., the metal atoms were also allowed to relax

from the constrained value of 2.77 Å. Calculations were conducted for π-bonded ethylene, di-σ-bonded ethylene, and ethylidyne species on Pt_{10} clusters and Pt_6Au_4 clusters. The Au atoms in the Pt_6Au_4 cluster were placed at the three corners of the 6-atom top layer and at the 1-atom bottom layer.

It is important to note that in both of the above scenarios for DFT calculations, the three-fold hollow site for ethylidyne adsorption comprised of three adjacent Pt atoms was preserved by the addition of Au. In this way, the DFT calculations probe the electronic effect of different atoms (i.e., Au atoms) surrounding the three-fold hollow site.

3. Results and discussion

Results from microcalorimetric measurements of H_2 adsorption on Pt/SiO_2 and $Pt/Au/SiO_2$ catalysts are displayed in figure 2. These data for the Pt/SiO_2 catalyst have been reported previously [5], and they are presented here for comparison with the behavior of the $Pt/Au/SiO_2$ catalysts. The Pt/SiO_2 and $Pt/Au/SiO_2$ catalysts had initial heats of hydrogen adsorption near 90 kJ/mol, in agreement with previous results for supported Pt catalysts [2,29]. The saturation H_2 uptakes on the Pt/SiO_2 and $Pt/Au/SiO_2$ catalysts correspond to Pt dispersions of approximately 60 and 55%, respectively.

XPS analysis indicated that there was no residual chlorine on the $Pt/Au/SiO_2$ catalyst. TEM analyses of the catalysts indicate that the average Pt particle size was between 2 and 5 nm on the Pt/SiO_2 catalyst. The particle size distribution was broader on the $Pt/Au/SiO_2$ catalyst, with a mixture of small (2–5 nm) particles and larger particles (up to 200 nm). Many of the larger particles appeared to be agglomerates of smaller particles. EDX analysis indicated that some of the larger particles contained primarily Au, while other particles contained both Pt and Au. An increase in particle size and the agglomeration of smaller particles into large particles has been reported when Au is added to Pt [12,21,30]. The only peaks observable in XRD scans of the $Pt/Au/SiO_2$ catalyst were from metallic Au particles. These results suggest that a fraction of the Au is present as large Au particles that are not associated with Pt.

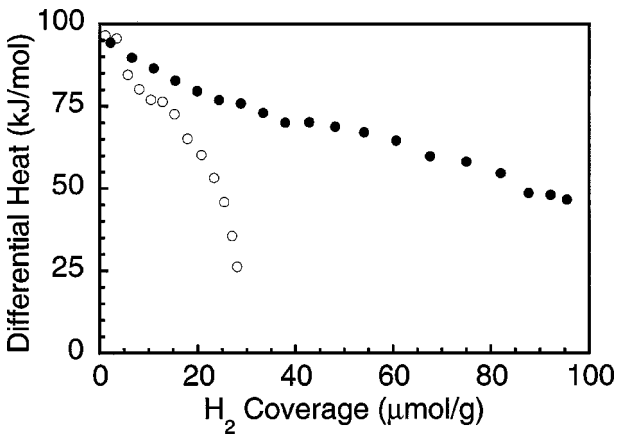

Figure 2. Differential heat versus adsorbate coverage for adsorption of H_2 at room temperature on Pt/SiO_2 (•) and $Pt/Au/SiO_2$ (○).

Figure 3 shows the results of microcalorimetric measurements of CO adsorption on the catalysts. The initial heat of CO adsorption on the Pt/SiO_2 and $Pt/Au/SiO_2$ catalysts was near 140 kJ/mol, which is in agreement with previous results on Pt/SiO_2 catalysts [2]. The initial heat of CO adsorption on the Au/SiO_2 sample was lower (70 kJ/mol). This result is in agreement with adsorption studies on Au/SiO_2, where it was found that CO uptakes were low and that essentially no irreversible adsorption occurred at 300 K [31]. Our low heat on Au/SiO_2 is in agreement with studies on Au films, where it was found that the uptake of CO was negligible [32]. The low CO coverage (2 μmol/g) on the Au/SiO_2 catalyst indicates that the sample had a poor metal dispersion.

Figure 3(b) shows the microcalorimetric results for CO adsorption, normalized by the corresponding saturation uptake of H atoms on the Pt/SiO_2 and $Pt/Au/SiO_2$ catalysts (the Au/SiO_2 catalyst did not adsorb H_2). The saturation CO/H ratio increased with the addition of Au. Also, the adsorption of CO is weaker on the $Pt/Au/SiO_2$ catalyst,

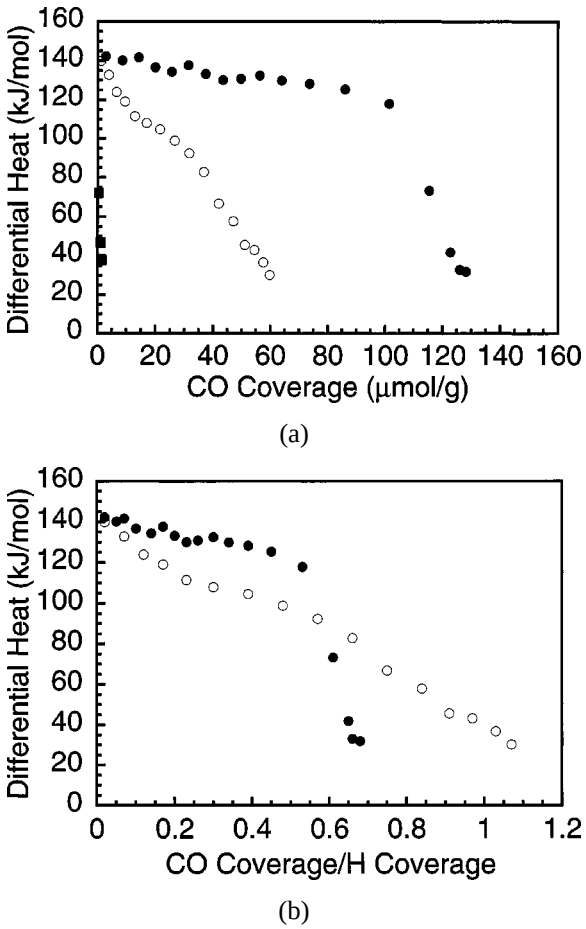

Figure 3. Differential heat versus (a) adsorbate coverage for CO adsorption at room temperature on Pt/SiO_2 (•), $Pt/Au/SiO_2$ (○), and Au/SiO_2 (■), and (b) CO coverage normalized by H coverage at room temperature on Pt/SiO_2 (•) and $Pt/Au/SiO_2$ (○).

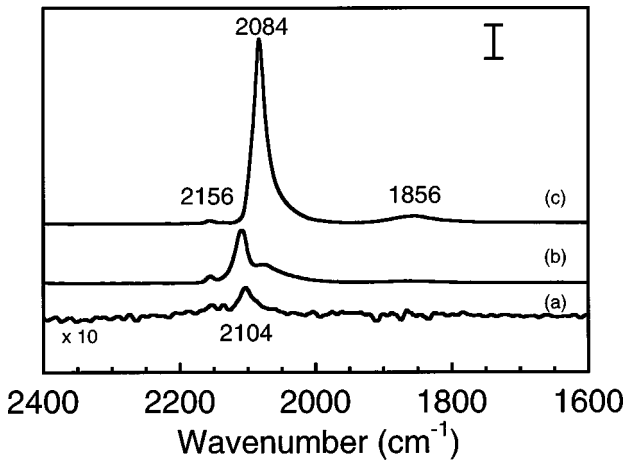

Figure 4. Infrared spectra for CO adsorption at 203 K with 3 Torr CO in the gas phase on (a) Au/SiO$_2$ (expanded 10×), (b) Pt/Au/SiO$_2$ and (c) Pt/SiO$_2$. The vertical bar corresponds to 0.4 absorbance units.

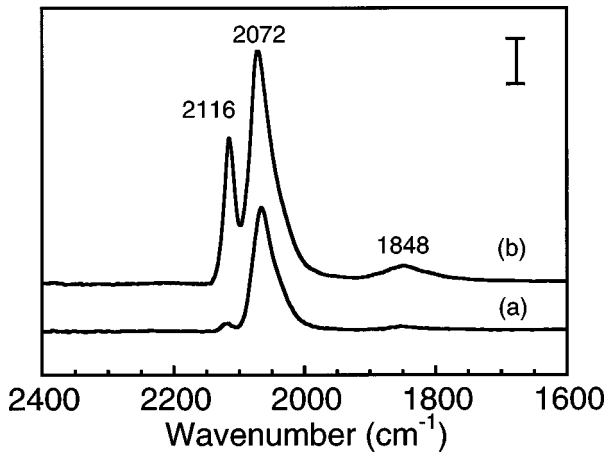

Figure 5. Infrared spectra for CO adsorption at room temperature on Pt/Au/SiO$_2$; (a) below saturation coverage with no gas-phase CO, and (b) at saturation coverage with 3 Torr CO in the gas phase. The vertical bar corresponds to 0.1 absorbance units.

especially at higher CO coverages. These results can be explained by the weak adsorption of CO on Au atoms, as described below in the analysis of IR spectra. It should be noted that a study on Pt/Au films indicated that exposure to CO can bring Pt to the surface [17]. The possibility of Pt surface enrichment on exposure to CO may, thus, affect the observed CO/H ratio. The isotherm for hydrogen uptake was collected at pressures up to only 3 Torr, and spillover of hydrogen to Au observed at higher pressures [33] should not be a factor.

Figure 4 presents IR spectra for CO adsorption on the Pt/SiO$_2$, Pt/Au/SiO$_2$ and Au/SiO$_2$ catalysts at 203 K. The bands near 2084 and 1856 cm^{-1} are from CO molecules adsorbed on atop and bridge sites of Pt atoms, respectively [34]. The weak band at 2156 cm^{-1} can be attributed to CO adsorbed on SiO$_2$, as confirmed by studies of CO adsorption on the SiO$_2$ support at low temperatures under conditions where gas-phase CO was present. The band near 2104 cm^{-1} can be assigned to CO adsorbed on Au sites [21,35,36]. Note that the intensity of the band for CO adsorbed on Au sites in figure 4, spectrum (b) for the Pt–Au/SiO$_2$ sample is about 50 times greater than the intensity of the band in figure 4, spectrum (a) for the Au/SiO$_2$ sample. Therefore, it can be concluded that the dispersion of gold was significantly increased by the presence of Pt in the Pt/Au/SiO$_2$ catalyst. DFT calculations for CO adsorption on three-atom Pt and Au clusters suggest that the extinction coefficients for CO adsorbed at atop sites on Pt and Au are similar. Therefore, the ratio of the corresponding peak intensities in figure 4, spectrum (b) indicates that there are more Au sites than Pt sites on the surface of the Pt/Au/SiO$_2$ catalyst.

Figure 5 shows IR spectra after CO adsorption at room temperature on the Pt/Au/SiO$_2$ catalyst. The bands at 2116 and 2072 cm^{-1} are for CO adsorbed on Au and Pt sites, respectively. The band at 1848 cm^{-1} is for CO adsorbed on bridge sites of Pt. At lower CO coverages (figure 5, spectrum (a)), the ratio of the band at 2116 cm^{-1} to the band at 2072 cm^{-1} is small and most of the adsorbed CO is thus associated with Pt. This IR result is consistent with the microcalorimetric result that the heat of CO adsorption is higher on Pt (140 kJ/mol) compared to Au (70 kJ/mol). At saturation coverage of CO on the Pt/Au/SiO$_2$ catalyst (figure 5, spectrum (b)), the ratio of the band intensities at 2116 and 2072 cm^{-1} has increased, indicating a significant extent of CO adsorption on Au. This behavior accounts for the higher CO/H ratio on the Pt/Au/SiO$_2$ catalyst than on the Pt/SiO$_2$ catalyst, as shown in figure 3(b). This weak adsorption of CO on Au atoms also accounts for the lower heats of CO adsorption on the Pt/Au/SiO$_2$ catalyst observed at high CO coverages.

In short, the results of our microcalorimetric and IR spectroscopic measurements of CO adsorption indicate that the Au is better dispersed on the Pt/Au/SiO$_2$ catalyst compared to the Au/SiO$_2$ catalyst. Therefore, it appears that even though large mono-metallic particles of Au exist on the Pt/Au/SiO$_2$ catalyst, as seen by TEM and XRD, there is significant interaction between Au and Pt. It is typical for Pt/Au catalysts to contain mixed Pt–Au particles and also to contain particles containing only Au [11,12,30]. To obtain a homogeneous Pt/Au alloy catalyst requires high-temperature calcination (e.g., 1000 K), but the resulting catalyst has particles with average diameters of 90 nm [37].

Comparison of the spectra (b) in figures 4 and 5 shows that the intensity of the band for CO on Au sites decreases with a corresponding increase in band intensity for CO on Pt sites upon warming from 203 K to room temperature. Generally the surfaces of Pt/Au alloys are enriched with Au [17,21,30,32,33,38,39]. However, it has been shown that the adsorption of CO may cause migration of Pt to the surface on Pt/Au catalysts [17]. Thus, we may suggest that Pt atoms become sufficiently mobile upon warming from 203 K to room temperature to become enriched at the surface of the Pt/Au/SiO$_2$ catalyst in the presence of CO.

Figure 6 shows the results of microcalorimetric measurements of ethylene adsorption on the Pt/Au/SiO$_2$ catalyst.

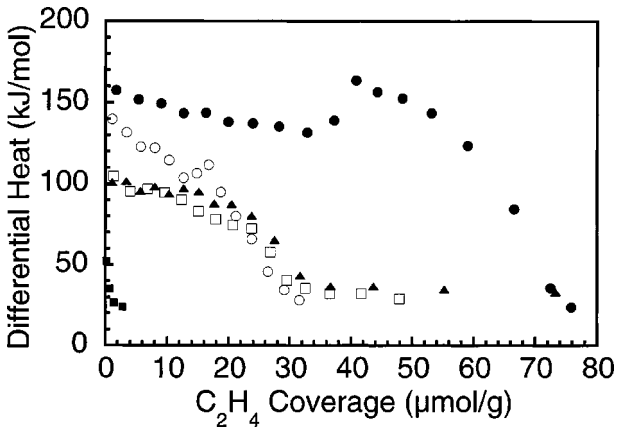

Figure 6. Differential heat versus adsorbate coverage for C_2H_4 adsorption on Pt/SiO_2 at 300 K (●), $Pt/Au/SiO_2$ at 300 K (○), $Pt/Au/SiO_2$ at 263 K (□), $Pt/Au/SiO_2$ at 203 K (▲), and Au/SiO_2 at 300 K (■).

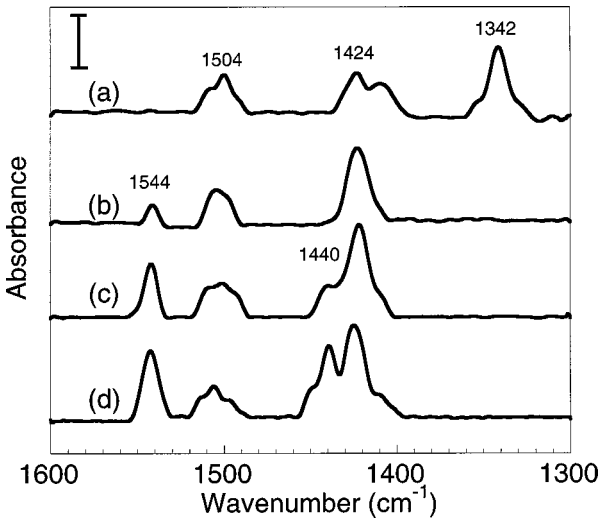

Figure 7. Infrared spectra for C_2H_4 adsorption on $Pt/Au/SiO_2$ at (a) 300, (b) 263, (c) 233, and (d) 203 K. The vertical bar corresponds to 0.001 absorbance units.

Also included on this figure, are the heat versus coverage curves for ethylene adsorption on Pt/SiO_2 and Au/SiO_2 at room temperature. Table 1 presents a summary of the initial heats of ethylene adsorption obtained in this study. Ethylene adsorption at room temperature produced an initial heat of 140 kJ/mol, which is lower than the value of 157 kJ/mol for the Pt/SiO_2 catalyst. An apparent maximum appears in the plot of differential heat versus coverage, because ethylene reacts with adsorbed hydrogen to produce gas-phase ethane. These hydrogen atoms are formed from the dissociative adsorption of ethylene to give ethylidyne species [6]. The curves of differential heat versus coverage are similar for the adsorption of ethylene on the $Pt/Au/SiO_2$ catalyst at 263 and 203 K, with initial heats of 105 and 100 kJ/mol, respectively; these values are lower than the values of 135 and 125 kJ/mol measured for the heat of ethylene adsorption on Pt/SiO_2 at temperatures of 263 and 203 K, respectively [5]. The plateau in the heat versus coverage at ca. 35 kJ/mol corresponds to ethylene adsorption on silica. The initial heat of adsorption on Au/SiO_2 was very low (ca. 50 kJ/mol).

Figure 7 shows IR spectra for ethylene adsorption on the $Pt/Au/SiO_2$ catalyst at temperatures from 203 K to room temperature. The IR spectrum (a) in figure 7 was collected at room temperature, and it shows bands at 1504, 1424, and 1342 cm^{-1}, corresponding to π-adsorbed ethylene, di-σ-adsorbed ethylene and ethylidyne species, respectively [5,40,41]. The shoulder near 1407 cm^{-1} is also from ethylidyne species [42]. For comparison, essentially only ethylidyne species are formed at room temperature on Pt/SiO_2 for the conditions of this study [5]. Thus, the π-bonded and di-σ-bonded ethylene species on the Pt/Au catalyst probably formed on Pt sites isolated by surrounding Au atoms, whereas ethylidyne species formed on sites with larger ensembles of surface Pt atoms. The significant decrease in the amount of ethylidyne species formed on the Pt/Au catalyst compared to the mono-metallic Pt catalyst is a strong indication that there is substantial interaction between Pt and Au for our $Pt/Au/SiO_2$ catalyst.

Spectrum (b) in figure 7 collected at 263 K shows only π-bonded and di-σ-bonded ethylene species, whereas ethylidyne species are also formed on Pt/SiO_2, at this temperature [5]. This behavior is further evidence for an interaction between Pt and Au, because ethylidyne species require three-fold hollow sites composed of adjacent Pt atoms. If there is interaction between Au and Pt, there will be fewer of these sites than on a Pt catalyst. Importantly, spectra (b), (c) and (d) of figure 7 also show a band at 1544 cm^{-1} that is not present for ethylene adsorption on Pt/SiO_2. In addition, this band was not present on $Pt/Sn/SiO_2$ catalysts [5]. Surface enhanced Raman scattering studies showed a band between 1535 and 1545 cm^{-1} for the coupled CH_2 scissor mode and C–C stretch mode of ethylene adsorbed on gold films and gold electrodes [43,44]. Therefore, we assign the band at 1544 cm^{-1} observed on our $Pt/Au/SiO_2$ sample to ethylene adsorbed on Au atoms. In fact, the IR spectra for CO adsorption at 203 K presented above showed that a significant number of Au sites are present on the surface of our $Pt/Au/SiO_2$ catalyst. The lower heats of ethylene adsorption on the $Pt/Au/SiO_2$ catalyst compared to the Pt/SiO_2 sample at 203 and 263 K may thus be attributed to the averaged contributions from ethylene adsorption on Pt atoms with the weaker adsorption of ethylene on Au atoms. The band near 1440 cm^{-1} in figure 7, spectra (c) and (d) corresponds to ethylene adsorption on silica [45].

Table 2 presents results for isobutane conversion over Pt/SiO_2 and $Pt/Au/SiO_2$ at 723 K for an isobutane pressure of 12.5 Torr, a hydrogen pressure of 75 Torr, and at a total pressure of 760 Torr (1 Torr = 133.33 Pa). The rates are taken after 1 min on stream before significant catalyst deactivation had occurred. Note that the thermodynamic equilibrium conversion at these conditions is 100% for hydrogenolysis, 60% for isomerization and 31% for dehydrogenation. The addition of Au to the Pt/SiO_2 catalyst leads to a slight decrease in the rate of hydrogenolysis, whereas

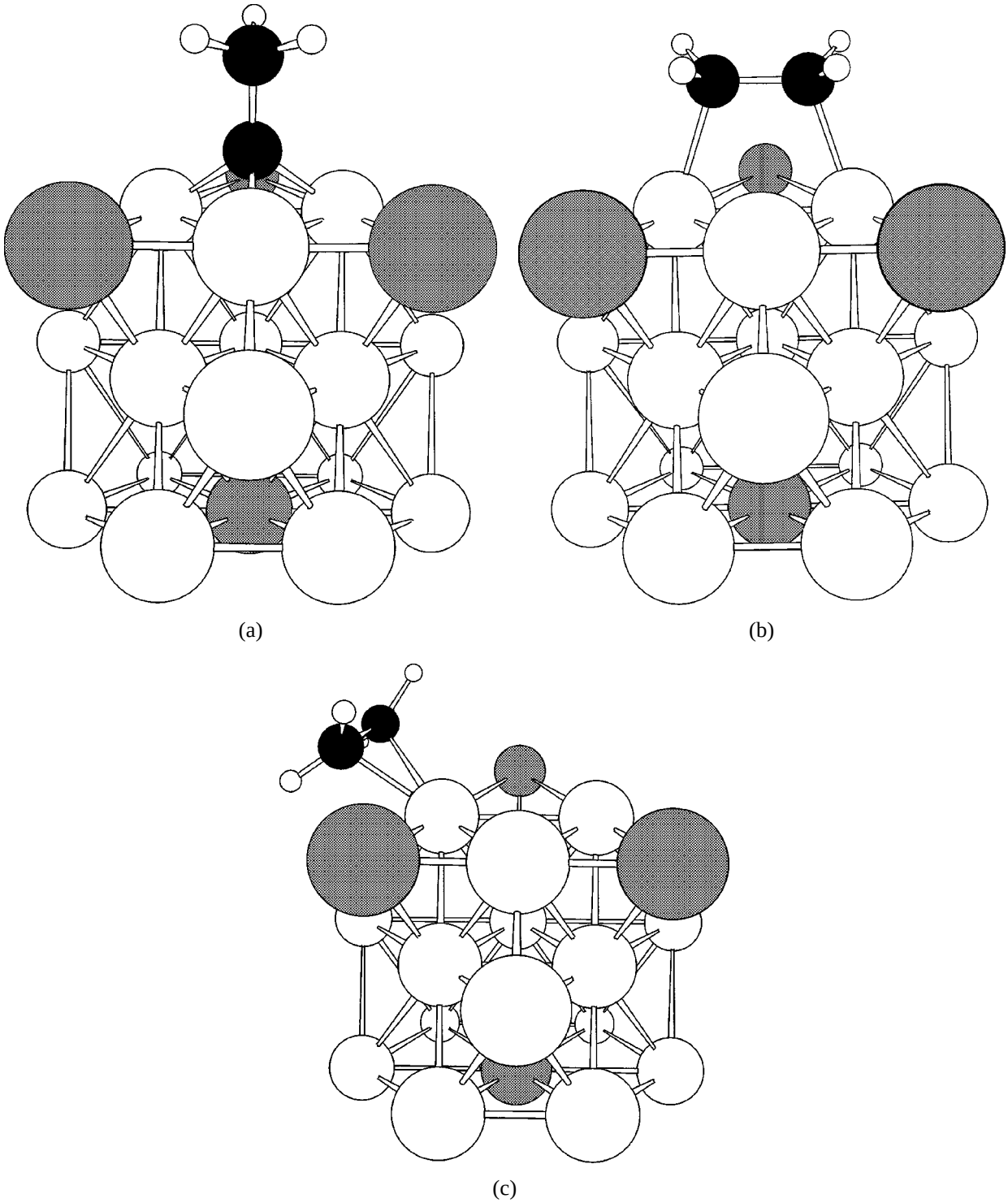

Figure 8. Ball and stick models of the structures used for DFT calculations – 19-atom cluster with (a) ethylidyne species, (b) di-σ-bonded ethylene and (c) π-bonded ethylene; large open circle = Pt atom; large shaded circle = Pt or Au atom; medium filled circle = C atom; small open circle = H atom.

the rates of n-butane production increase upon addition of Au. Schwank and co-workers [12,13] have shown that the addition of Au to Pt-based catalysts causes the rates of isomerization to increase and the rates of hydrogenolysis to decrease for reactions of n-hexane and neopentane. They suggest that the addition of Au decreases the size of the surface Pt ensembles, where large ensembles of Pt atoms favor hydrogenolysis reactions and small ensembles would favor isomerization. Sachtler and Somorjai [15] also observed on a Pt(111) surface that the addition of Au increased the isomerization rate of n-hexane and it decreased the hydrogenolysis and aromatization rates. For comparison with these results for Pt/Au/SiO$_2$, we have reported previously that the addition of Sn to Pt/SiO$_2$ decreases the rates of

Table 2
Isobutane conversion over Pt and Pt/Au catalysts at 723 K, 12.5 Torr isobutane, 75 Torr hydrogen, and 760 Torr total pressure.

	Catalyst	
	Pt/SiO_2	$Pt/Au/SiO_2$
WHSV (h^{-1})[a]	38	31
iC_4H_{10} conversion (%)	30	22
Hydrogenolysis TOF (1/s)[b]	0.15	0.12
n-C_4H_{10} TOF (1/s)	0.03	0.1
iC_4H_8 TOF (1/s)	0.17	0.59
Conversion to iC_4H_8 (%)	15	15

[a] WHSV = (g isobutane/h)/(g catalyst).
[b] Hydrogenolysis TOF = $(1/4)(CH_4$ TOF + $2(C_2H_6$ TOF) + $3(C_3H_8$ TOF)).

Table 3
Changes in electronic energies (kJ/mol) for adsorption calculated for π-, di-σ-, and ethylidyne species on Pt_{19}, $Pt_{15}Au_4$, Pt_{10}, and Pt_6Au_4 clusters.

Catalyst	π-species	Di-σ-species	Ethylidyne + $(1/2)H_{2(g)}$
19-atom cluster[a]			
Pt_{19}	−71	−116	−94
$Pt_{15}Au_4$	−60	−100	−137
Difference of heat	−11	−16	43
10-atom cluster[b]			
Pt_{10}	−103	−149	−109
Pt_6Au_4	−102	−135	−160
Difference of heat	−1	−13	51

[a] Pt–Pt and Pt–Au distances are fixed at their bulk value of 2.77 Å.
[b] Pt and Au atoms are allowed to relax by conducting optimization of the entire cluster.

Table 4
Mulliken populations on Pt atoms involved in the adsorption in 5d and 6sp bands.

Cluster	Pt 6sp[a]	Pt 5d[a]
Pt_{10}	3.27	26.67
Pt_6Au_4	2.78	26.80
Pt_6Sn_4	4.05	27.51

[a] This population is the sum for the three Pt atoms comprising the three-fold hollow site.

hydrogenolysis and isomerization reactions for isobutane conversion [1–4].

Figure 8 shows ethylidyne species, di-σ-bonded ethylene and π-bonded ethylene associated with the 19-atom cluster. The results from our DFT calculations for ethylene adsorption on 19-atom and 10-atom metal clusters containing Pt and Au are shown in table 3. The addition of Au to Pt leads to essentially no change in the heat of formation of π-adsorbed and di-σ-adsorbed ethylene on $Pt_{15}Au_4$ and Pt_6Au_4 clusters compared to Pt_{19} and Pt_{10} clusters, respectively. Table 4 shows the Mulliken populations on Pt atoms involved in the adsorption of ethylene. The addition of Au to Pt leads to a lower population of the 6sp orbital of Pt (by 0.49 electrons) and higher population of the 5d orbital (by 0.13 electrons). The Pauli repulsion interactions between occupied levels are proportional to the adsorbate coordination number and the square of the overlap between the adsorbate orbital and the metal atomic orbital. To a first approximation, the Pauli repulsion is proportional to the number of Pt–C bonds, but the overlap term may cause the effect to be non-linear. We note that the C atom is situated closer to the metal surface in a three-fold site than it is in a two-fold or atop site. As a result, the Pauli repulsion interactions are more important for bonding on high-coordination metal sites, such as three-fold hollow sites on which ethylidyne species form, than for bonding on lower coordination metal sites, such as atop and bridge sites on which π-bonded and di-σ-bonded ethylene species form [46]. Therefore, the lower electron density on the Pt atoms caused by donation of electrons from Pt to Au should have a greater effect on the formation of ethylidyne species than on the formation of π-bonded and di-σ-bonded ethylene species.

We have shown earlier that the addition of Sn to Pt leads to higher populations of the 6sp and 5d orbitals of Pt [5], and this behavior is also summarized in table 4. In contrast to this effect of Sn, we find that the addition of Au to Pt leads to a lower population of the 6sp orbital of Pt and higher population of the 5d orbital (see table 4). There is a net electron transfer from Pt to Au in Pt/Au clusters, whereas electrons are transferred from Sn to Pt in Pt/Sn clusters. This observation is in agreement with the Pauling electronegativities for these elements, which are 2.2, 2.4 and 1.8 for Pt, Au and Sn, respectively.

In our previous DFT studies of ethylene interaction with Pt and Pt/Sn clusters [5], we found that Sn donates electrons to Pt and weakens the interaction of ethylidyne species with three-fold hollow sites comprised of adjacent Pt atoms. In the present paper, our calculations indicate that Au withdraws electrons from Pt and leads to a more attractive interaction between Pt and ethylidyne species. Therefore, it appears from these calculations that Au and Sn have rather different effects on the formation of ethylidyne species on Pt. Specifically, the addition of Sn to Pt suppresses the formation of ethylidyne species by a geometric effect (i.e., decreasing the number of three-fold hollow sites comprised of adjacent Pt atoms) and by exerting an electronic effect (i.e., decreasing the heat of interaction of ethylidyne species with three-fold hollow sites comprised of adjacent Pt atoms surrounded by Sn). However, the addition of Au to Pt may suppress the formation of ethylidyne species only by exerting a geometric effect, since Au may actually increase the heat of interaction of ethylidyne species with three-fold hollow sites comprised of adjacent Pt atoms surrounded by Au. The results of these calculations are in agreement with calculations by Neurock [47] on Pd/Au clusters, in which it was found that Au had primarily a geometric effect in the activation of C–H bonds.

4. Conclusions

The initial heats for ethylene adsorption on $Pt/Au/SiO_2$ were 140, 105 and 100 kJ/mol at 300, 263 and 203 K, respectively. These heats are lower than the heats on Pt/SiO_2,

because the addition of Au inhibits the formation of ethylidyne species at 300 and 263 K by reducing the size of the surface Pt ensembles (i.e., a geometric effect), and also because ethylene adsorbs on Au sites at 263 and 203 K with a lower heat of adsorption.

The quantum chemical calculations indicate that Au exerts a smaller electronic effect on Pt than does the addition of Sn to Pt. In fact, the addition of Au to Pt slightly increases the heat of formation of ethylidyne species on a three-fold hollow site comprised of three adjacent Pt atoms surrounded by Au atoms (Pt/Au cluster), whereas the addition of Sn to Pt significantly decreases the heat of formation of ethylidyne species on a three-fold hollow site comprised of three adjacent Pt atoms surrounded by Sn atoms (Pt/Sn cluster).

Acknowledgement

We wish to acknowledge funding from the National Science Foundation. The TEM analysis was performed at the Materials Science Center of the University of Wisconsin (UW), which receives partial support from the NSF-Materials Research Science and Engineering Center (MRSEC) at the UW. The Natural Sciences and Engineering Research Council of Canada provided a graduate scholarship for JMH.

References

[1] J.M. Hill, R.D. Cortright and J.A. Dumesic, Appl. Catal. A 168 (1998) 9.
[2] R.D. Cortright and J.A. Dumesic, J. Catal. 148 (1994) 771.
[3] R.D. Cortright and J.A. Dumesic, Appl. Catal. A 129 (1995) 101.
[4] R.D. Cortright, D. Bergene, P. Levin, M. Natal-Santiago and J.A. Dumesic, in: *11th International Conference of Catalysis – 40th Anniversary* (1996) p. 1185.
[5] J. Shen, J.M. Hill, R.M. Watwe, B.E. Spiewak and J.A. Dumesic, J. Phys. Chem. B (1999), accepted.
[6] B.E. Spiewak, R.D. Cortright and J.A. Dumesic, J. Catal. (1998), in press.
[7] M.T. Paffett, S.C. Gebhard, R.G. Windham and B.E. Koel, Surf. Sci. 223 (1989) 449.
[8] Y.L. Tsai, C. Xu and B.E. Koel, Surf. Sci. 385 (1997) 37.
[9] H. Verbeek and W.M.H. Sachtler, J. Catal. 42 (1976) 257.
[10] J.K.A. Clarke, A.C.M. Creaner and T. Baird, Appl. Catal. 9 (1984) 85.
[11] J. Schwank, K. Balakrishnan and A. Sachdev, Stud. Surf. Sci. Catal. 75 (1993) 905.
[12] A. Sachdev and J. Schwank, J. Catal. 120 (1989) 353.
[13] K. Balakrishnan and J. Schwank, J. Catal. 132 (1991) 451.
[14] J.R.H. van Schaik, R.P. Dessing and V. Ponec, J. Catal. 38 (1975) 273.
[15] J.W.A. Sachtler and G.A. Somorjai, J. Catal. 81 (1983) 77.
[16] K. Foger and J.R. Anderson, J. Catal. 61 (1980) 140.
[17] R. Bowman and W.M.H. Sachtler, J. Catal. 19 (1970) 127.
[18] F.J.C.M. Toolenaar, D. Reinalda and V. Ponec, J. Catal. 64 (1980) 110.
[19] L.-C. de Ménorval, A. Chaqroune, B. Coq and F. Figueras, J. Chem. Soc. Faraday Trans. 93 (1997) 3715.
[20] K. Balakrishnan and J. Schwank, J. Catal. 138 (1992) 491.
[21] K. Balakrishnan, A. Sachdev and J. Schwank, J. Catal. 121 (1990) 441.
[22] B.E. Spiewak, J. Shen and J.A. Dumesic, J. Phys. Chem. 99 (1995) 17640.
[23] B.E. Spiewak and J.A. Dumesic, Thermochim. Acta 290 (1996) 43.
[24] *Jaguar*, J. Schrödinger, Inc., Portland, OR (1998).
[25] A.D. Becke, J. Chem. Phys. 98 (1993) 5648.
[26] P.J. Hay and W.R. Wadt, J. Chem. Phys. 82 (1985) 299.
[27] W.J. Hehre, L. Radom, P.V.R. Schleyer and J.A. Pople, in: *Ab Initio Molecular Orbital Theory* (Wiley, New York, 1987).
[28] R.M. Watwe, B.E. Spiewak, R.D. Cortright and J.A. Dumesic, Catal. Lett. 51 (1998) 139.
[29] S.B. Sharma, J.T. Miller and J.A. Dumesic, J. Catal. 148 (1994) 198.
[30] S. Galvagno and G. Parravano, J. Catal. 57 (1979) 272.
[31] S. Lin and M.A. Vannice, Catal. Lett. 10 (1991) 47.
[32] J.J. Stephan, V. Ponec and W.M.H. Sachtler, Surf. Sci. 47 (1975) 403.
[33] J.R. Anderson, K. Foger and R.J. Breakspere, J. Catal. 57 (1979) 458.
[34] C. De La Cruz and N. Sheppard, Spectrochim. Acta A 50 (1994) 271.
[35] J. France and P. Hollins, J. Electron Spectrosc. Relat. Phenom. 64/65 (1993) 251.
[36] E.L. Kugler and M. Boudart, J. Catal. 59 (1979) 201.
[37] J.K.A. Clarke, A.F. Kane and T. Baird, J. Catal. 64 (1980) 200.
[38] H.C. de Jongste, F.J. Kuijers and V. Ponec, in: *Preparation of Catalysts*, eds. B. Delmon et al. (Elsevier, Amsterdam, 1976) p. 207.
[39] L. Guczi, J. Mol. Catal. 25 (1984) 13.
[40] N. Sheppard and C. De La Cruz, Adv. Catal. 41 (1996) 1.
[41] N. Sheppard and C. De La Cruz, Adv. Catal. 42 (1998) 1.
[42] S.B. Mohsin, M. Trenary and H.J. Robota, J. Phys. Chem. 92 (1988) 5229.
[43] Ü. Ertürk and A. Otto, Surf. Sci. 179 (1987) 163.
[44] M.L. Patterson and M.J. Weaver, J. Phys. Chem. 89 (1985) 1331.
[45] G. Busca, G. Ramis, V. Lorenzelli, A. Janin and J.C. Lavalley, Spectrochim. Acta A 43 (1987) 489.
[46] R.A. van Santen and M. Neurock, Catal. Rev. Sci. Eng. 37 (1995) 557.
[47] M. Neurock, in: *Dynamics of Surfaces and Reaction Kinetics in Heterogeneous Catalysis*, Vol. 109, eds. G.F. Froment and K.C. Waugh (Elsevier, New York, 1997) p. 3.